# Cornered silver and silver–platinum nanodisks: Preparation and promising activity for alkaline oxygen reduction catalysis

Chien-Liang Lee[*], Ciou-Mei Syu, Chun-Han Huang, Hsueh-Ping Chiou, Yi-Ju Chao, Chia-Chen Yang

*Department of Chemical and Materials Engineering, National Kaohsiung University of Applied Sciences, Kaohsiung 807, Taiwan*

## ABSTRACT

A simple method for the efficient synthesis of cornered Ag and Ag–Pt nanodisks by using triangular Ag nanoplates as reactants has been developed. The triangular Ag nanoplates are heated and reshaped to spherical nanodisks; in turn, through the introduction of $PtCl_4^{2-}$ ions, the spherical nanodisks undergo sculpturing and a subsequent displacement reaction to form cornered Ag nanodisks and Ag–Pt nanodisks with pores. The selected-area electron diffraction pattern shows that the cornered Ag nanodisks are composed of two basal Ag (1 1 1) planes, thus indicating the occurrence of selective etching on the spherical nanodisks by this method. The analyses provided by X-ray diffraction spectroscopy and line-scanned energy-dispersive spectroscopy confirm the compositions of these cornered nanodisks and the mixed alloy in the Ag–Pt nanodisks. For the investigation of the practical feasibility of the application of the proposed method, these cornered Ag and Ag–Pt nanodisks were then used as methanol-tolerant electrocatalysts in the alkaline oxygen reduction reaction (ORR). Electrochemical measurements were performed using an ultrathin-film rotating ring-disk electrode. The two types of nanodisks are found to have high stabilities and improved activities in 1 M NaOH electrolyte. In the electrolyte with free methanol, the mass activities at −0.1 V (vs. Ag/AgCl; within kinetic control region) in terms of the currents normalized to Ag mass for the Ag nanodisks and Ag–Pt nanodisks are $6.98 \times 10^{-4}$ and $2.01 \times 10^{-3}$ mA μg$^{-1}$, respectively, which are greater than the value of $2.09 \times 10^{-4}$ mA μg$^{-1}$ for Ag nanoparticles. The order in terms of the ORR activity is found to be as follows: cornered Ag–Pt nanodisks > cornered Ag nanodisks > Ag nanoparticles. Additionally, in the presence of methanol, all the cornered nanodisk catalysts experience cathodic currents, indicating that the ORR occurs despite the use of a methanol solution.

© 2012 Elsevier B.V. All rights reserved.

## 1. Introduction

The oxygen reduction reaction (ORR) is now at its limit in alkaline fuel cells, which are environmentally friendly and promising energy sources owing to their low pollution and high energy densities. Typically, Pt is now the most commonly used ORR catalyst [1–8], but some discoveries [9–13] indicate that excessively strong binding between $O_2$ and the Pt surface would lead to relatively unfavorable removal of $OH_{ads}$, which is one probable reason for the slow kinetics [9], and thus, the loss of cell voltage [14]. In addition to the electrochemical factor, the high cost of pure Pt catalysts is also an issue for the ongoing commercialization of such fuel cells. With these problems in mind, it is clear that new catalysts still need to be developed.

Inexpensive Ag nanomaterials, including spherical nanoparticles [15–17], nanowires [18,19], and triangular nanoplates [20],

are currently attracting considerable attention as electrocatalysts in alkaline ORRs because they have higher stability than pure Pt cathodes for long-term operation, even if their activities are lower than those of Pt catalysts [16]. On the basis of studies conducted using a catalytic model, it was suggested that increasing the number of active sites on the catalyst surface [21–23] or alloying [24–26] would help improve the electrochemical activity. One important strategy for increasing the active site area is the use of the cornered catalysts, which can provide unsaturated atoms or islands for reaction with the reactant during catalysis. Narayanan [27] and Mahmoud [28] reported the exquisite reaches in which the activation energy of one electron-transfer reaction between thiosulfate and hexacyanoferrate (III) is shape-dependent owing to the promotion of more highly active nanocatalysts with more corners and edges. Recently, Zhang and co-workers [29] further decorated isolated Au atoms on one Pd nanocluster to provide active sites and enhance aerobic glucose oxidation. The alloying of Ag catalysts is another option for increasing their kinetics for the ORR. In a previous report [30], it was mentioned that the bonding between Ag and $O_2$ is considerably weaker than that between Pt and $O_2$. This

* Corresponding author. Tel.: +886 7 3814526x5131; fax: +886 7 3830674.
*E-mail addresses:* cl_lee@cc.kuas.edu.tw, cl_lee@url.com.tw (C.-L. Lee).

leads to the difficult breaking of the O—O bond on the Ag surface. Therefore, in order to produce a stronger Ag—$O_2$ bond, and consequently, lead to easier breaking of the O—O bond, an alteration and increase in the d-band center position of Ag observed from the plot of the d-band center energy and kinetic current density has been suggested [31]. From this point of view, for the development of new types of catalysts, the Ag catalyst is often alloyed with Pt [24,32], which results in a stronger binding ability for $O_2$. This technique can also efficiently reduce the amount of Pt used.

Our previous study showed that triangular Ag nanoplates (≈136 nm) with three corners led to an ORR with an electron number of approximately 3.16, as determined by rotating disk electrode experiments and the Koutecky–Levich equation [20]. It was reported that the corners of these triangular nanoplates are more active than the basal and edge planes [33]. Through measurements conducted using a rotating ring-disk electrode (RRDE), an $OH^-$ production efficiency of >80% was determined for the ORR using these triangular nanoplates as the electrocatalyst in a 1 M NaOH electrolyte [34]. Herein, we develop a simple method for the synthesis of cornered Ag nanodisks and porous derivatives alloyed with Pt through the heating and sculpture of triangular nanoplates using $PtCl_4^{2-}$ ions. The composition ratio of Pt to Ag in the nanodisks can increase with increasing displacement time in the Pt salt solution. These novel cornered nanodisks are tested for their potential as catalysts in ORRs in the presence and absence of methanol. The ORR activities and kinetics in term of the mass current densities ($j_m$) for these novel cornered nanodisks are compared to those of the triangular nanoplates.

## 2. Experimental

### 2.1. Synthesis and material analysis of hexagonal nanoplates, Ag nanoparticles and Pt nanoparticles

The 140-nm-sized triangular Ag nanoplates as reactants were synthesized using a modified seed-growth method, which has previously been reported elsewhere [34], to increase the yield. A solution of the synthesized triangular Ag nanoplates (3 mL) was precipitated by centrifugation at 4000 rpm, and redispersed using 3 mL of deionized water to reduce the interaction of free hexadecyltrimethyl ammonium bromide during the displacement period. Next, the Ag nanoplate solution was heated for 20 min at a constant temperature of 60 °C. Approximately 25 μL of $1.11 \times 10^{-2}$ M $K_2PtCl_4$ solution ($2.78 \times 10^{-7}$ moles) was added to 3 mL of a well-stirred solution of triangular Ag nanoplates at a constant temperature of 60 °C. After 20 min, cornered Ag nanodisks were obtained. Hollow Ag—Pt nanodisks with corners were obtained when the reaction time was prolonged to 70 min. In order to draw a fair comparison between the electrochemical properties of cornered nanodisks, Ag nanoparticles and Pt nanoparticles were prepared. The synthesis of Ag nanoparticles was based on the previous report [35], where Ag nanoparticles protected by hexadecyltrimethyl ammonium ions were obtained. As to the synthesis of Pt nanoparticles, 1 mL of a 0.01 M $K_2PtCl_6$ aqueous solution was added to 10 mL of a 0.1 M hexadecyltrimethyl ammonium bromide aqueous solution at a fixed temperature of 95 °C. Then, 0.2 mL of a 0.2 M $NaBH_4$ was gradually added to the mixed solution with stirring for 1 min and aging for 30 min at 95 °C. A dark brown Pt nanoparticle solution was then obtained.

The prepared nanodisk solutions were dropped onto copper grids and allowed to dry naturally; then, their compositions, characteristic shapes, and sizes were measured and observed using line-scanned energy-dispersive X-ray spectroscopy (LS-EDX) combined with transmission electron microscopy (TEM; JEOL JEM-3000F). The optical properties of these cornered nanodisks

prepared from Ag nanoplates, such as their surface plasmon resonance (SPR), were determined using a UV-vis spectrophotometer (Agilent 8453). The X-ray diffraction (XRD) patterns of the prepared nanodisks were obtained using XRD spectroscopy (Shimadzu XD-3A, Cu anode).

### 2.2. Electrochemical measurements

The electrochemical activities of the prepared cornered nanodisks for use in cyclic voltammetry (CV) or polarization curve experiments were evaluated by performing RRDE measurements. First, a solution containing $4 \times 10^{-2}$ mg of the Ag, Ag—Pt or Pt catalyst and 3 μL of 5% Nafion was dropped onto a 0.196-$cm^2$ GCE disk, which was then heated to 50 °C to evaporate the water. The amount of nanodisk powder coated on the GCE was confirmed by quartz-crystal microbalance measurements. RRDE measurements were performed using a combination of an RRDE system (AFMSRCE, Pine Co., Ltd.) and a bipotentiostat (CHI 727D). A nanodisk-modified rotating glassy carbon disk/platinum ring electrode (ring area: 0.11 $cm^2$) was used as the working electrode. In addition, a Pt counter electrode and a Ag/AgCl (3 M KCl; 0.210 V vs. NHE) reference electrode were used for polarization measurements in $N_2$- or $O_2$-saturated 1 M $NaOH_{(aq)}$ solution with or without 0.5 M methanol. The disk potential was varied from 0 to −0.7 V, whereas the ring potential was maintained at 0.145 V to oxidize the $HO_2^-$ produced by $O_2$ reduction at the disk electrode.

## 3. Results and discussion

Fig. 1A–E shows sequential TEM images of the microstructures of nanoparticles prepared by heating the Ag nanoplate solution at 60 °C and subsequently introducing $PtCl_4^{2-}$ ions. Initially, with the selective adsorption of hexadecyltrimethyl ammonium ions as an additive in a seed solution to block the seed surface and govern the growth direction on nanoplates in the growth pathway [34], nanoplates as seen in Fig. 1A were prepared, with their SPR spectrum shown in Fig. 2. The statistical results for the nanoplate shapes are shown in Fig. 3A. ~79.04% of the nanoplates are triangular, and the mean edge length of these triangular nanoplates is approximately 140 nm. After heating this solution in which the triangular nanoplates of Fig. 1A were dispersed, the triangular shapes of the nanoplates changed to spherical disk or obtuse forms, as shown in Fig 1B. On the basis of the information in the TEM image of Fig. 1B and the shape distribution shown in Fig. 3B, it is found that 64.72% and 31.64% of the nanoparticles are spherical nanodisks and obtuse triangle nanoplates, respectively. Several studies [33,36] have indicated that triangular nanoplates can become smaller but thicker disk-like nanoplates when the nanoplate solution is heated above 40 °C. The corresponding SPR peak located at long wavelength (584 nm), assigned to the in-plane dipole resonance, is quickly blue-shifted [36]. In this case, as a comparison in Fig. 2, a significant in-plane dipole peak shifting from 808 nm (triangular nanoplates) to 681 nm (spherical nanodisks and obtuse nanoplates) was observed with the reduction in basal size, as seen in Fig. 1B. Interestingly, many hexagonal nanodisks as detected in Fig. 1C are obtained by adding $PtCl_4^{2-}$ ions to the heated nanoplate solution for 20 min. From this TEM result (Fig. 1C), the shape distribution of nanodisks was calculated, and is shown in Fig. 3C. A greater change in nanodisk shape can be seen from Fig. 3B and C. The percentage of hexagonal nanodisks with six corners increases from approximately zero to 74.09%, and the percentage of irregular nanodisks with corners is 23.78%. On the basis of the statistical result (Fig. 3C) from the TEM image of Fig. 1C, it is found that the obtuse triangular nanoplates have almost disappeared. It is known that triangular Ag nanoplates are very sensitive to halogen ions [37],
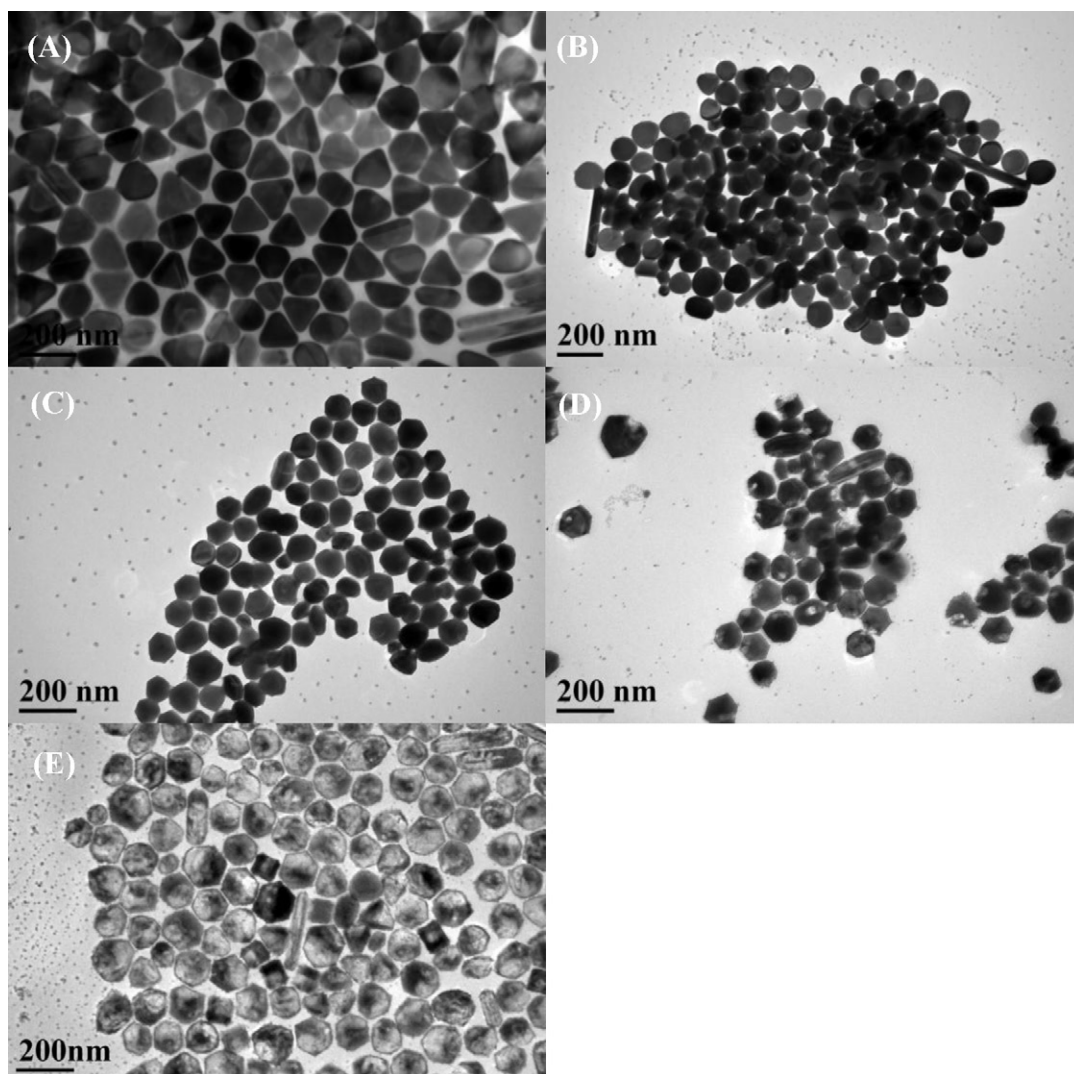
**Fig. 1.** Time-resolved TEM images in the formation of cornered nanodisks. (A) Original nanoplates, (B) after 20 min heating at 60 °C, (C) after 20 min with introduction of $K_2PtCl_4$ at 60 °C, (D) after 40 min with introduction of $K_2PtCl_4$ at 60 °C, and (E) after 70 min with introduction of $K_2PtCl_4$ at 60 °C.

and the corners and (1 1 0) side facets can be etched further by chloride ions to form nanodisks [38–40]. Tang and co-workers [39] successfully demonstrated interesting results in which the etch ability of $Cl^- < I^- < Br^-$ for silver nanoplates was determined. The
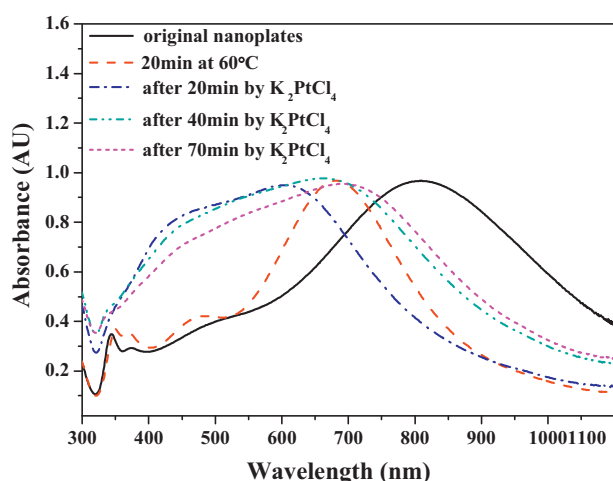


**Fig. 2.** Time-resolved SPR optics for the formation of cornered nanodisks.

facet-dependent etching of the $PtCl_4^{2-}$ complex toward nanoplates was found in this study. In order to analyze the microstructure of the hexagonal solid nanodisks (Fig. 1C), the electron beam of a high-resolution TEM was employed to focus on a single nanodisk, as captured in Fig. 4A. From the top, an almost flat top plane but rough edge planes were observed. With magnification, perfect atomic arrangement on the top plane (Fig. 4B) was detected. Fig. 4C shows the selected-area electron diffraction (SAED) pattern obtained using an electron beam focused on a specific area of this single nanoplate. The diffraction pattern reveals very bright spots with six-fold symmetry, which are assigned to the {2 2 0} reflections of a face-centered cubic (fcc) single crystal orientated in the [1 1 1] direction. This data indicates that the flat nanoplate surface is parallel to the (1 1 1) plane. The parallel (1 1 1) plane detected in the SAED pattern can reasonably be assumed to result from the top and bottom basal planes of this single hexagonal nanoplate. It was evident that the two basal planes of the as-synthesized Ag nanoplates are (1 1 1) facets [41–43]. Therefore, from these images and the SAED pattern, $PtCl_4^{2-}$ could be concluded to be more inactive on these top and bottom (1 1 1) planes during the formation of cornered nanodisks. Interestingly, broad long-wavelength SPR peak was detected for the cornered Ag nanodisks, as shown in Fig. 2. This is attributed to the in-plane dipole SPR of the unequilateral basal plane of most of the nanodisks, as detected in Fig. 1C.
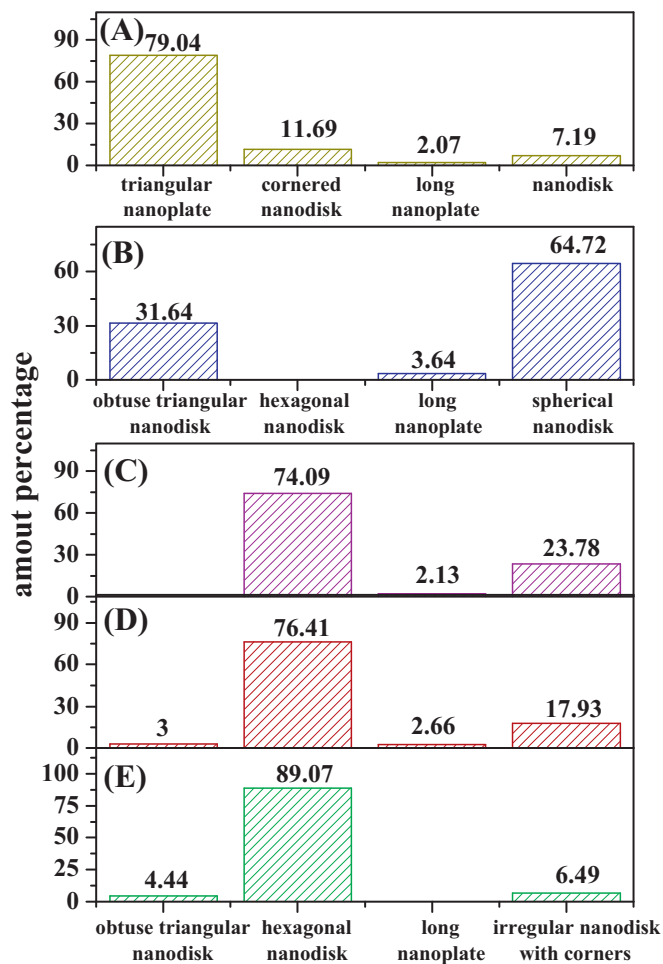
**Fig. 3.** Statistical results on the morphology and percentage of nanoparticles in Fig. 1A–E. (A) Original nanoplates, (B) after 20 min heating at 60 °C, (C) after 20 min with introduction of $K_2PtCl_4$ at 60 °C, (D) after 40 min with introduction of $K_2PtCl_4$ at 60 °C, and (E) after 70 min with introduction of $K_2PtCl_4$ at 60 °C.

Furthermore, as a consequence of $PtCl_4^{2-}$ addition, in Fig. 1D and E, an expanding pinhole and a hollowing-out condition were observed in the TEM images of the nanodisks reacted with $PtCl_4^{2-}$ for 40 and 70 min, respectively. Of the nanoparticles shown in Fig. 1D and E, 76.41% and 89.07% are hexagonal nanodisks, as shown in Fig. 3D and E, respectively, and 17.93% and 6.49% are irregular nanodisks with corners, respectively. A percentage of cornered nanodisks of more than 95% indicates that the shapes of these nanodisks were almost maintained but that their insides were hollowed out when the synthesis time was increased. In order to detect the composition architecture of the hollow cornered nanodisks (Fig. 1E), SAED and XRD analyses were employed. Fig. 5B presents the SAED pattern obtained by electron diffraction of a single hollow cornered nanodisk with pores, as shown in the image in Fig. 5A. The four spots in the pattern are ascribed to the light diffractions in the Ag (1 1 1), Ag (2 0 0), Ag (2 2 0), and Ag (3 1 1) planes. Simultaneously, two bright spots of Pt (2 2 0) and Pt (3 1 1) are observed. Not only Ag but also Pt is present in this cornered nanodisks, focused by the electron beam of TEM. Fig. 6 further shows a comparative XRD spectrum of these hollow nanodisk powders and their template powders, the hexagonal cornered nanodisks (Fig. 1C), which were prepared with $PtCl_4^{2-}$ for 20 min. First, four peaks located at 38.08°, 44.28°, 64.35°, and 77.32° detected from the dry hexagonal nanodisk powder are assigned as the (1 1 1), (2 0 0), (2 2 0), and (3 1 1) diffraction planes of the fcc structure, respectively. These peaks, confirmed by the Ag standard spectrum
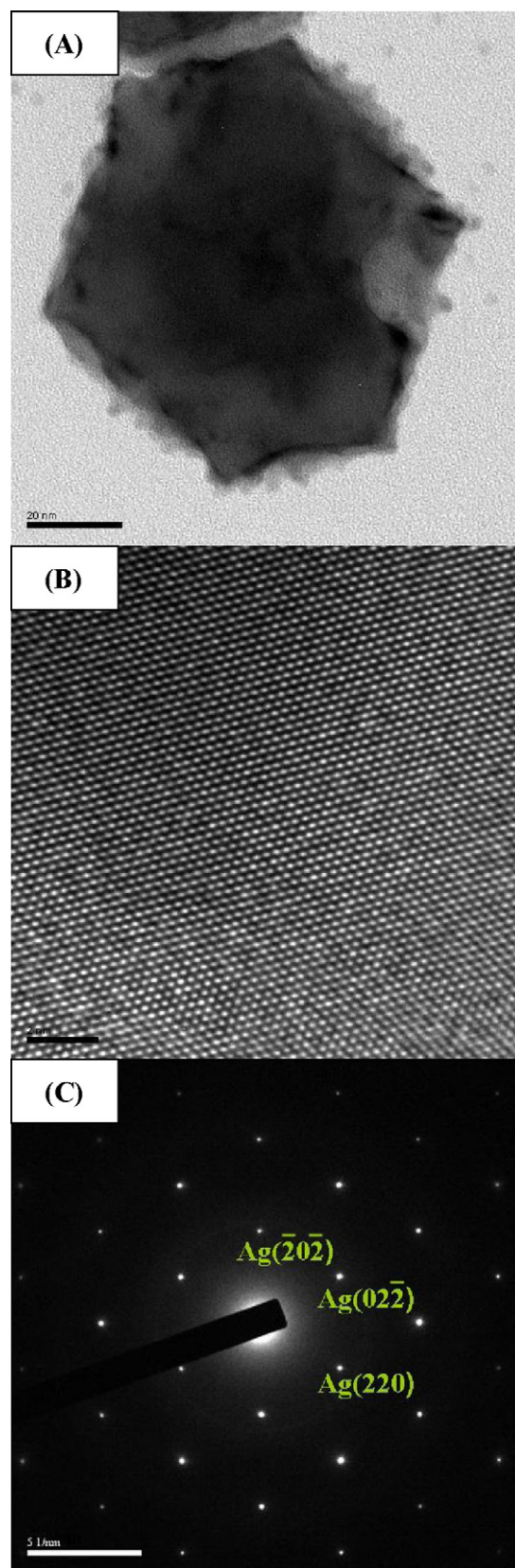


**Fig. 4.** High-resolution TEM images and SAED pattern of single cornered Ag nanodisk. (A) TEM image of single nanodisk, (B) high-resolution TEM image of (1 1 1) plane located at the top of nanodisk, and (C) SAED pattern.
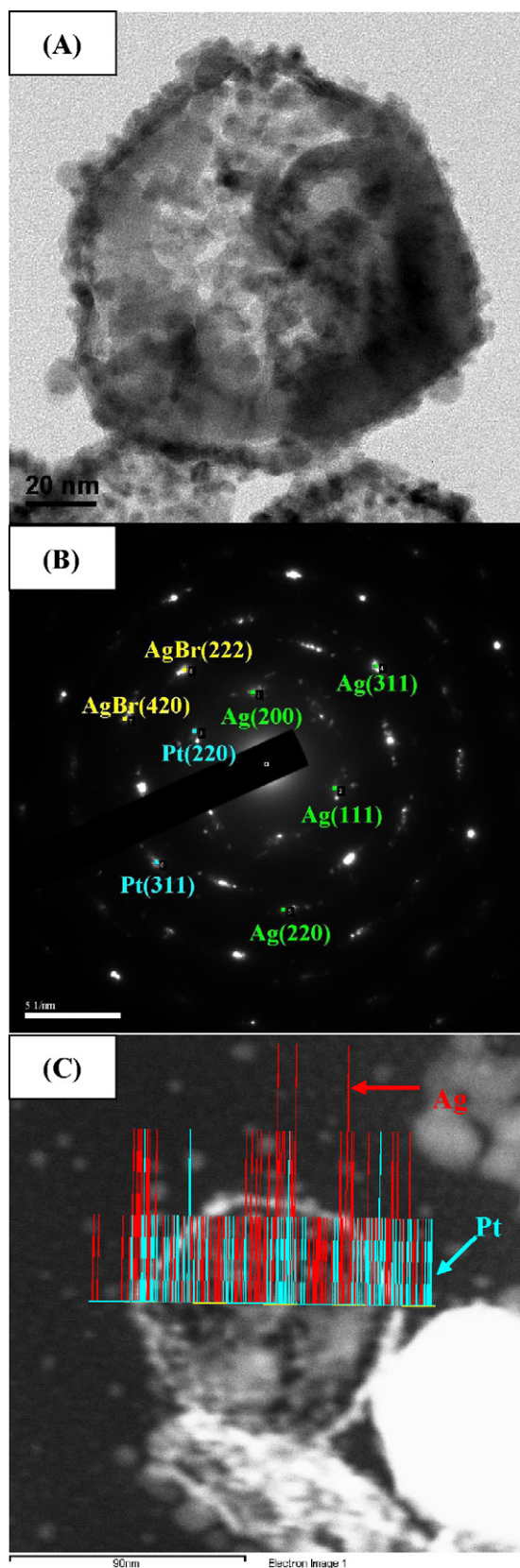
**Fig. 5.** TEM images, SAED pattern, and LS-EDX result of single cornered Ag–Pt nanodisk. (A) TEM image of single nanodisk, (B) SAED pattern, and (C) LS-EDX results.
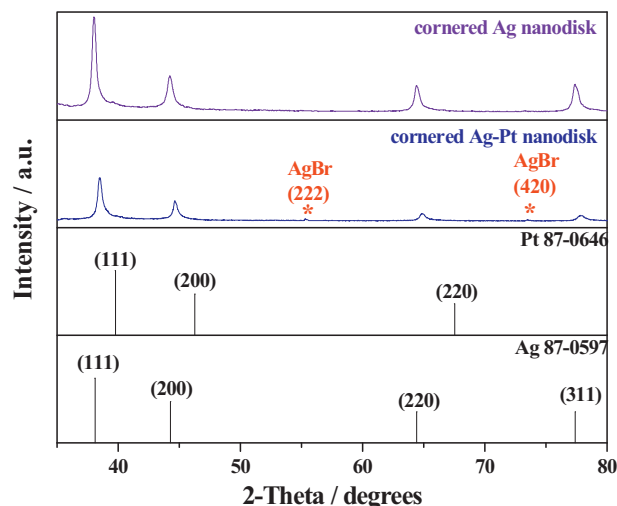


**Fig. 6.** Comparative XRD patterns of the cornered Ag and Ag—Pt nanodisks (*symbol for AgBr).

(JCPDS No. 087-0597), suggest that Ag nanodisks were not deposited with Pt in the induction period of 20 min after the addition of $PtCl_4^{2-}$. This indicates that in the induction period, the spherical nanodisks were sculptured to hexagonal nanodisks or irregular nanodisks with corners. Compared with the XRD pattern of the hexagonal Ag nanodisks, the diffraction peaks located at 38.41°, 44.70°, 64.73°, and 77.81° detected from the dry hollow nanodisk powders shift to the standard spectrum of Pt. This indicates that these cornered Ag nanodisks were deposited by Pt via a displacement method and that they were composed of a Ag—Pt alloy, as confirmed by the SAED result shown in Fig. 5B. In this displacement reaction, AgBr, as identified in the XRD and SAED patterns (Fig. 5B), was formed through the reaction of hexadecyltrimethylammonium bromide (protecting agent) and Ag⁺ dissolved from the nanodisks. Additionally, Fig. 5C presents the LS-EDX spectrum of hollow nanodisks, as the image of the cornered nanodisk was captured. The two strong and uniform signals from the hollow nanomaterials identify them as Ag and Pt, suggesting that a mixed alloy formed in the nanodisk walls. In these solid walls, Ag and Pt account for 79.3% and 20.7%, respectively, in weight percentages; the atomic percentages of Ag and Pt are 87.48% and 12.62%, respectively. This platinum deposition also resulted in a red shift of the SPR peak, as shown in the comparative spectra (Fig. 2) of the hexagonal Ag nanodisks reacted with $PtCl_4^{2-}$.

Fig. 7 shows the overall path for the formation of hexagonal Ag nanodisks and hollowed Ag—Pt nanodisks with corners and pores. First, triangular Ag nanoplates were heated and transformed to nanodisks because of the instability of the nanoplate corners. Hexagonal or cornered nanodisks were formed by the etching of chloride ions. Then, the displacement reaction began between the cornered nanodisks and Pt²⁺. Holes were formed and gradually expanded, making the disks hollow; simultaneously, metallic Pt was deposited on the nanodisk surfaces, and finally, hollow Ag—Pt nanodisks with corners and pores were created.

The feasibility of using these cornered Ag and Ag—Pt nanodisks as electrocatalysts toward alkaline ORRs was then examined. Their electrochemical properties were initially measured by CV. Fig. 8A shows a comparison of the CV curves obtained by measuring the electrochemical responses of the cornered Ag nanodisks in 1 M $NaOH_{(aq)}$ solution under N₂ and O₂ atmospheres. In N₂, the shoulder response for the oxidation current at 0.09 V (vs. Ag/AgCl) is like the initial stage of Ag nanodisk oxidation and dissolution [44]. A subsequent current at 0.163 V is associated with the formation of a $Ag_2O$ monolayer, while the strong redox pair of $E = 0.2$ V and
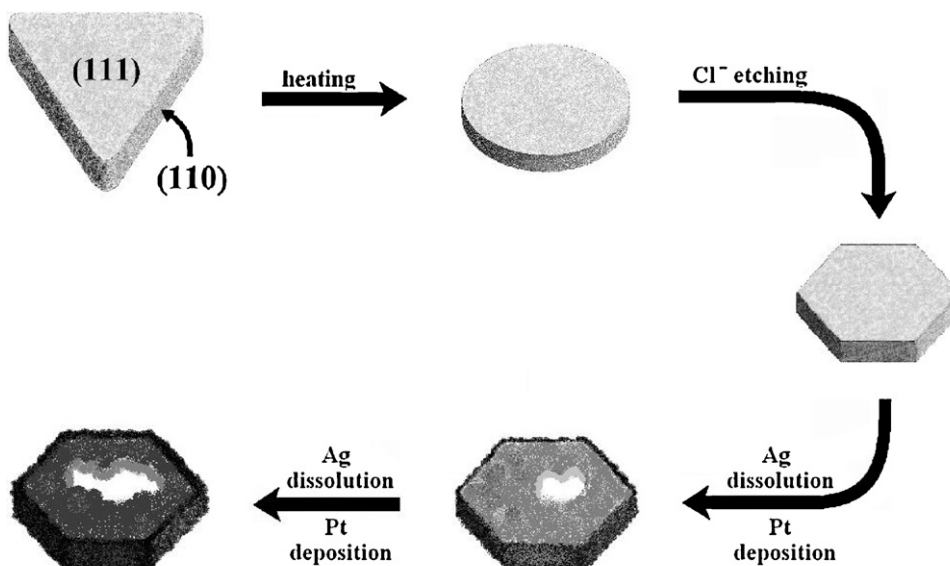
**Fig. 7.** Illustration of the formation of cornered Ag—Pt and Ag nanodisks from triangular Ag nanoplates.

0.125 V is attributed to bulk $Ag_2O$ formation and reduction [45]. When $O_2$ gas is pumped into the electrolyte, the peak positions for initial Ag oxidation and the $Ag_2O$ monolayer shift slightly to 0.086 V and 0.156 V, respectively, which indicates that the oxidation occurs earlier. Notably, the intensity and the area of the redox pair of bulk $Ag_2O$ are not altered upon $O_2$ saturation. This indicates that the real surface areas of the cornered Ag nanodisks are not easily changed owing to their stability in the $O_2$ medium. Interestingly, not only the area, but also the position of the $Ag_2O$ redox pair as seen in Fig. 8B for hollow Ag—Pt nanodisks in the $N_2$ and $O_2$ surrounding is equal. The surface roughness on Ag—Pt catalysts cannot be altered, even if dosing $O_2$. The hollow Ag—Pt nanodisks show a higher stability during electrocatalysis. This means that the additional trace Pt can stabilize these Ag-based catalysts during the ORR.

A further comparison of the CV curves of Fig. 8A and B in $N_2$ and $O_2$ shows that the significant reduction currents attributed to the
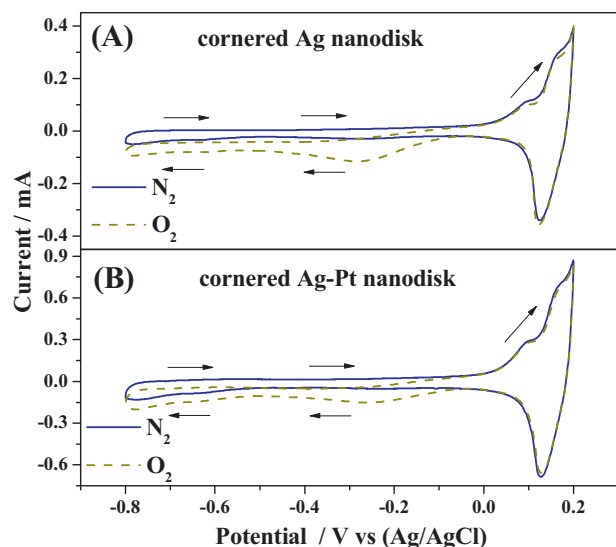
catalysis of $O_2$ reduction from −0.07 V (vs. Ag/AgCl) mean that the cornered Ag and Ag—Pt nanodisks have activity toward ORRs.

The electrochemical activity and kinetic properties of these novel catalysts compared to those of triangular nanoplates were studied using RRDE experiments. Fig. 9 shows polarization curves for the $O_2$ reduction catalyzed by cornered Ag nanodisks, Ag—Pt nanodisks, triangular Ag nanoplates, Ag nanoparticles and Pt nanoparticles dispersed on the disk electrode, wherein the $HO_2^-$ production was determined by in situ measurement using a Pt ring electrode at 0.145 V (vs. Ag/Ag/Cl) in the 1 M $NaOH_{(aq)}$ solution. The morphologies of the 7.7 nm Pt and 35.6 nm Ag nanoparticles used in this analysis are confirmed by TEM images, as shown in the insets of Fig. 9. In terms of the disk current with cornered Ag nanodisks, the currents limited by kinetic control and diffusion control are obtained before −0.1 V and after −0.3 V, respectively. The
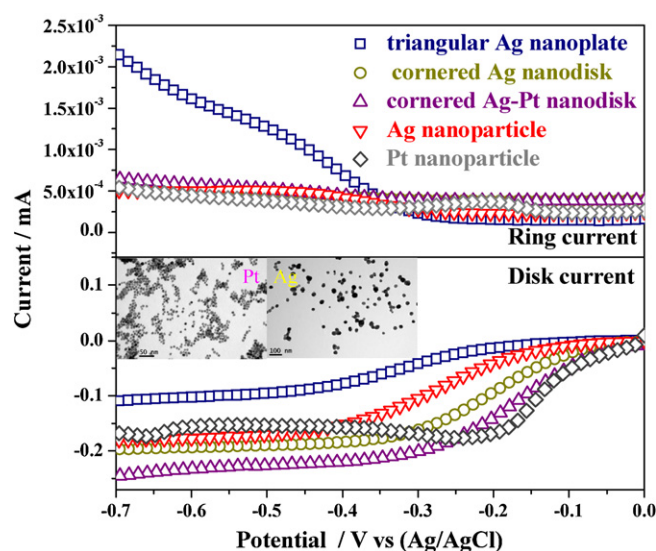


**Fig. 8.** Comparative CV curves of cornered Ag and Ag—Pt nanodisks in $N_2$-saturated and $O_2$-saturated 1 M NaOH electrolyte. Scan rate: 50 mV s$^{-1}$. Electrolyte temperature: 25 °C.



**Fig. 9.** Polarization curves obtained using RRDE measurements for triangular Ag nanoplates, cornered Ag nanodisks, cornered Ag—Pt nanodisks, Ag nanoparticles and Pt nanoparticles in $O_2$-saturated 1.0 M NaOH electrolyte. Scan rate: 10 mV s$^{-1}$. Electrode rotation speed: 500 rpm. Electrolyte temperature: 25 °C. (Insets: TEM images of Ag and Pt nanoparticles.)
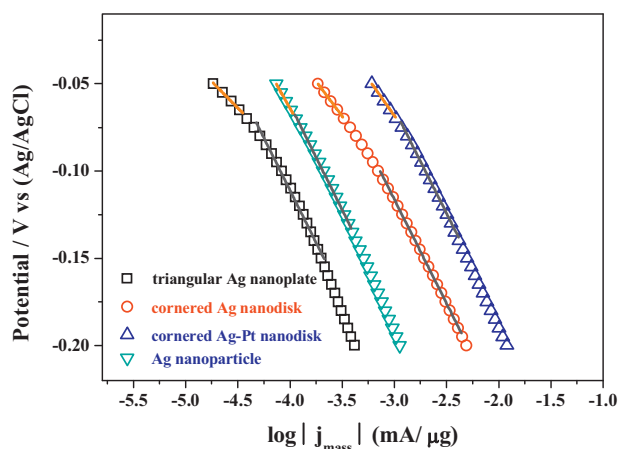
**Fig. 10.** Comparative Tafel plots normalized to the mass of Ag loading in a free methanol electrolyte.

current between −0.1 and −0.3 V is determined by both kinetic and diffusion factors. Compared with the disk current of the cornered Ag nanodisks, a longer region at $E > -0.15$ V attributed to kinetic control for the triangular nanoplates indicates slower ORR kinetics. For the cornered Ag and Ag—Pt nanodisks, a significant disk current ($I_d$) is obtained, and an almost negligible ring current ($I_r$) is observed, whereas the opposite result is obtained for triangular Ag nanoplates, especially with the linear increase in $I_r$ after −0.35 V (within the diffusion-control region). Additionally, the ratios of the ring to disk current densities at −0.1 V for the cornered Ag nanodisks, Ag—Pt nanodisks, Ag nanoplates, Ag nanoparticles, and Pt nanoparticles are $2.86 \times 10^{-2}$, $1.37 \times 10^{-2}$, $8.19 \times 10^{-2}$, $4.53 \times 10^{-2}$, and $7.96 \times 10^{-3}$, respectively. Thus, a ratio order of Ag nanoplate $\gg$ Ag nanoparticle > cornered Ag nanodisk > hollow Ag—Pt nanodisk > Pt nanoparticle is obtained. This result suggests that the cornered nanodisks are efficient catalysts that induce a low yield of $HO_2^-$ during the ORR period except for Pt nanoparticles.

For a precise comparison of the mass activities of these novel Ag-based catalysts and Ag nanoparticles, the ORR kinetic currents normalized to the mass ($j_m$) of the silver catalyst are plotted in Fig. 10. Typically, $j_m$ can be estimated by [46]:

$$j_m = \frac{(i_d \times i)/(i_d - i)}{L_{Ag}}$$

where $i_d$ is the diffusion-limiting current at −0.4 V in this study (controlled at 25 °C), and $L_{Ag}$ is the Ag loading weight. As shown in the Tafel curve for the triangular Ag nanoplates (Fig. 10), two different linear Tafel slopes of −60 mV dec$^{-1}$ and −120 mV dec$^{-1}$ were observed for low and high overpotentials, respectively. The two slopes can be explained in terms of $O_2$ coverage, by the Temkin isotherm (high coverage) at low overpotentials and the Langmuir isotherm (low coverage) at high overpotentials. For Ag nanoparticles, cornered Ag nanodisks, Ag—Pt nanodisks, the slopes at high overpotentials were also −120 mV dec$^{-1}$. Interestingly, the Tafel slopes at low overpotentials changed to −80 mV dec$^{-1}$ and −85 mV dec$^{-1}$ for the catalysts of cornered Ag nanodisks and Ag—Pt nanodisks, indicating that the shape and composition of these plate-like catalysts could influence the initial adsorption behavior of $O_2$. In a comparison, at −0.1 V (vs. Ag/AgCl), the $j_m$ values of the cornered Ag, Ag—Pt nanodisks, Ag nanoplates and Ag nanoparticles were $6.98 \times 10^{-4}$ mA μg$^{-1}$, $2.01 \times 10^{-3}$ mA μg$^{-1}$, $8.3 \times 10^{-5}$ mA μg$^{-1}$, and $2.09 \times 10^{-4}$ mA μg$^{-1}$, respectively. Thus, an activity order of hollow Ag—Pt nanodisk > cornered Ag nanodisk > Ag nanoparticle > Ag nanoplate is obtained. It is reported that the activity of carbon powder-supported Ag nanoparticles
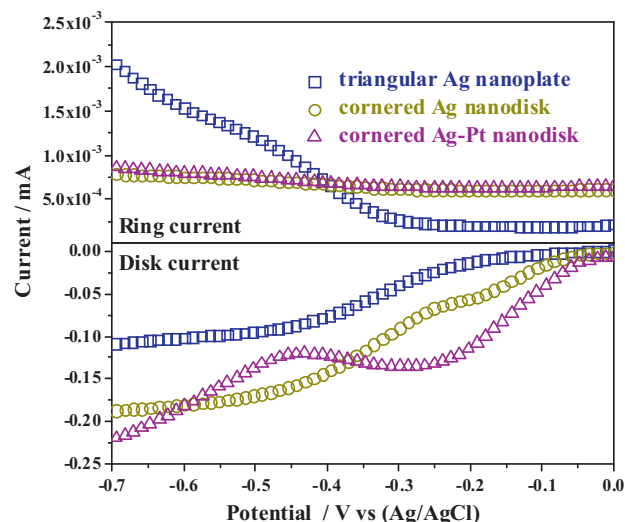


**Fig. 11.** Polarization curves obtained using RRDE measurements for triangular Ag nanoplates, cornered Ag nanodisks, and cornered Ag—Pt nanodisks in $O_2$-saturated 0.5 M methanol/1 M NaOH electrolyte. Scan rate: 10 mV s$^{-1}$. Electrode rotation speed: 500 rpm. Electrolyte temperature: 25 °C.

(Ag/C) can reach to $3.37 \times 10^{-4}$ mA μg$^{-1}$ in a 1-M KOH electrolyte [47]. In a comparison with Ag/C catalysts, the cornered Ag—Pt and Ag nanodisks without needed carbon supports show higher activities to produce fast kinetics toward the ORR.

It is well known that the crossover of methanol from the anode to the Pt cathode can decrease the cell potential. A competitive reaction therefore occurs between the ORR and methanol oxidation, necessitating methanol tolerance of the electrocatalyst. For further evaluation of the ORR activity in a methanol-containing electrolyte, Fig. 11 compares the polarization curves of the prepared cornered Ag nanodisks, Ag—Pt nanodisks, and triangular Ag nanoplates measured by RRDE under a NaOH electrolyte with 0.5 M methanol in an $O_2$ atmosphere. As the depiction of the disk current curve of Fig. 11 illustrates, the cornered Ag and Ag—Pt nanodisks both experienced cathodic currents, which indicates that ORRs occurred even in the presence of methanol. This result leads to the conclusion that these cornered nanodisks are suitable for use as methanol-tolerant catalysts in the alkaline ORR. According to the report about the use of Ag and Pt catalysts for ORR [16], the anodic currents from the location of potential > 0.8 V vs. reversible hydrogen electrode are observed in the interference of 0.5 M methanol. As recent, in the pathway of methanol oxidation by Ag [48] and Pt—Ag [49] catalysts, the necessity and promotion of silver oxides on the surface of these catalysts are evaluated. The information about cathodic currents in the whole potential region provided by Fig. 11 indicates that these cornered catalysts are not oxidized during preparation. The similar feature for the base ORR property was observed in the Ag/MnyOx catalyst [50].

Comparison of the ratio of the current densities on the ring to the disk at −0.1 V further indicates whether a higher or lower $HO_2^-$ concentration is produced during the ORR in the presence of methanol using these novel catalysts. These ratios for the cornered Ag nanodisks, Ag—Pt nanodisks, and Ag nanoplates are $6.28 \times 10^{-2}$, $2.64 \times 10^{-2}$, and $11.6 \times 10^{-2}$, respectively. In a comparison with the ratios measured in the ORR without methanol, increases of approximately $3.42 \times 10^{-2}$ from the ratios for the two Ag catalysts and a smaller increase of about $1.27 \times 10^{-2}$ for the cornered Ag—Pt nanodisks are found. These results indicate that the $HO_2^-$ concentration increases slightly in the ORR with methanol, in which the cornered Ag—Pt nanodisk produces the minimum $HO_2^-$ concentration.

## 4. Summary

Cornered Ag nanodisks and Ag—Pt nanodisks with pores were prepared by a simple reaction in which the added $PtCl_4^{2-}$ reacts slowly with the prepared triangular Ag nanoplates at 60 °C. Improved electrocatalytic properties of these cornered nanodisks in ORRs were identified. The activities at −0.1 V (within the kinetic-control region) in terms of mass current density for the Ag nanodisks and Ag—Pt nanodisks were $6.98 \times 10^{-4}$ mA μg$^{-1}$ and $2.01 \times 10^{-3}$ mA μg$^{-1}$, which are greater than the activity of $8.3 \times 10^{-5}$ mA μg$^{-1}$ for Ag nanoplates. These cornered nanodisks can be used successfully as electrocatalysts in the ORR, even in the presence of methanol.

## Acknowledgements

## References

[1]  E. Antolini, E.R. Gonzalez, Journal of Power Sources 195 (2010) 3431.
[2]  J.S. Spendelow, A. Wieckowski, Physical Chemistry Chemical Physics 9 (2007) 2654.
[3]  M. Zhiani, H.A. Gasteiger, M. Piana, S. Catanorchi, International Journal of Hydrogen Energy 36 (2011) 5110.
[4]  H.A. Gasteiger, S.S. Kocha, B. Sompalli, F.T. Wagner, Applied Catalysis B: Environmental 56 (2005) 9.
[5]  N.R. Elezovic, B.M. Babic, P. Ercius, V.R. Radmilovic, L.M. Vracar, N.V. Krstajic, Applied Catalysis B: Environmental 125 (2012) 390.
[6]  T. Kottakkat, A.K. Sahu, S.D. Bhat, P. Sethuraman, S. Parthasarathi, Applied Catalysis B: Environmental 110 (2011) 178.
[7]  D. Sebastian, A. Garcia Ruiz, I. Suelves, R. Moliner, M. Jesus Lazaro, V. Baglio, A. Stassi, A.S. Arico, Applied Catalysis B: Environmental 115 (2012) 269.
[8]  S. Zhang, Y. Shao, G. Yin, Y. Lin, Applied Catalysis B: Environmental 102 (2011) 372.
[9]  D.H. Lim, J. Wilcox, The Journal of Physical Chemistry C 116 (2012) 3653.
[10]  A.B. Anderson, Electrochimica Acta 47 (2002) 3759.
[11]  V. Stamenkovic, B.S. Mun, K.J.J. Mayrhofer, P.N. Ross, N.M. Markovic, J. Rossmeisl, J. Greeley, J.K. Norskov, Angewandte Chemie International Edition 45 (2006) 2897.
[12]  T. Toda, H. Igarashi, H. Uchida, M. Watanabe, Journal of Electrochemical Society 146 (1999) 3750.
[13]  M.H. Shao, A. Peles, K. Shoemaker, Nano Letters 11 (2011) 3714.
[14]  A.A. Gewirth, M.S. Thorum, Inorganic Chemistry 49 (2010) 3557.
[15]  J.S. Guo, A. Hsu, D. Chu, R.R. Chen, The Journal of Physical Chemistry C 114 (2010) 4324.
[16]  L. Demarconnay, C. Coutanceau, J.M. Leger, Electrochimica Acta 49 (2004) 4513.
[17]  P. Singh, D.A. Buttry, The Journal of Physical Chemistry C 116 (2012) 10656.
[18]  K. Ni, L. Chen, G.X. Lu, Electrochemistry Communications 10 (2008) 1027.
[19]  M.A. Kostowskyj, R.J. Gilliam, D.W. Kirk, S.J. Thorpe, International Journal of Hydrogen Energy 33 (2008) 5773.
[20]  C.L. Lee, H.P. Chiou, C.M. Syu, C.C. Wu, Electrochemistry Communications 12 (2010) 1609.
[21]  Z.M. Peng, H. Yang, Journal of American Chemical Society 131 (2009) 7542.
[22]  Y.W. Lee, M. Kim, Y. Kim, S.W. Kang, J.H. Lee, S.W. Han, The Journal of Physical Chemistry C 114 (2010) 7689.
[23]  S.W. Lee, S.O. Chen, W.C. Sheng, N. Yabuuchi, Y.T. Kim, T. Mitani, E. Vescovo, Y. Shao-Horn, Journal of American Chemical Society 131 (2009) 15669.
[24]  T.C. Nagaiah, A. Maljusch, X.X. Chen, M. Bron, W. Schuhmann, Chemphyschem 10 (2009) 2711.
[25]  M. Chatenet, M. Aurousseau, R. Durand, F. Andolfatto, Journal of Electrochemical Society 150 (2003) D47.
[26]  S. Schwamborn, L. Stoica, W. Schuhmann, Chemphyschem 12 (2011) 1741.
[27]  R. Narayanan, M.A. El-Sayed, Nano Letters 4 (2004) 1343.
[28]  M.A. Mahmoud, C.E. Tabor, M.A. El-Sayed, Y. Ding, Z.L. Wang, Journal of American Chemical Society 130 (2008) 4590.
[29]  H.J. Zhang, T. Watanabe, M. Okumura, M. Haruta, N. Toshima, Nature Materials 11 (2012) 49–52.
[30]  F.H.B. Lima, J.F.R. de Castro, E.A. Ticianelli, Journal of Power Sources 161 (2006) 806.
[31]  F.H.B. Lima, J. Zhang, M.H. Shao, K. Sasaki, M.B. Vukmirovic, E.A. Ticianelli, R.R. Adzic, The Journal of Physical Chemistry C 111 (2007) 404.
[32]  F.H.B. Lima, C.D. Sanches, E.A. Ticianelli, Journal of Electrochemical Society 152 (2005) A1466.
[33]  B. Tang, J. An, X.L. Zheng, S.P. Xu, D.M. Li, J. Zhou, B. Zhao, W.Q. Xu, The Journal of Physical Chemistry C 112 (2008) 18361.
[34]  C.L. Lee, C.M. Syu, H.P. Chiou, C.H. Chen, H.L. Yang, International Journal of Hydrogen Energy 36 (2011) 10502.
[35]  C.L. Lee, H.P. Chiou, C.M. Syu, C.R. Liu, C.C. Yang, C.C. Syu, International Journal of Hydrogen Energy 36 (2011) 12706.
[36]  S.H. Chen, Z.Y. Fan, D.L. Carroll, The Journal of Physical Chemistry B 106 (2002) 10777.
[37]  X.C. Jiang, A.B. Yu, Langmuir 24 (2008) 4300.
[38]  S.P. Xu, B. Tang, X.L. Zheng, J. Zhou, J. An, X.H. Ning, W.Q. Xu, Nanotechnology 20 (2009) 7.
[39]  B. Tang, S.P. Xu, J. An, B. Zhao, W.Q. Xu, J.R. Lombardi, Physical Chemistry Chemical Physics 11 (2009) 10286.
[40]  J. An, B. Tang, X.L. Zheng, J. Zhou, F.X. Dong, S.P. Xu, Y. Wang, B. Zhao, W.Q. Xu, The Journal of Physical Chemistry C 112 (2008) 15176.
[41]  S.H. Chen, D.L. Carroll, Nano Letters 2 (2002) 1003.
[42]  D. Aherne, D.M. Ledwith, M. Gara, J.M. Kelly, Advanced Functional Materials 18 (2008) 2005.
[43]  V. Germain, J. Li, D. Ingert, Z.L. Wang, M.P. Pileni, The Journal of Physical Chemistry B 107 (2003) 8717.
[44]  J.M.M. Droog, C.A. Alderliesten, P.T. Alderliesten, G.A. Bootsma, Journal of Electroanalytical Chemistry 111 (1980) 61.
[45]  M. Hepel, M. Tomkiewicz, Journal of Electrochemical Society 131 (1984) 1288.
[46]  K.J.J. Mayrhofer, D. Strmcnik, B.B. Blizanac, V. Stamenkovic, M. Arenz, N.M. Markovic, Electrochimica Acta 53 (2008) 3181.
[47]  S. Maheswari, P. Sridhar, S. Pitchumani, Electrocatalysis 3 (2012) 13.
[48]  G. Orozco, M.C. Perez, A. Rincon, C. Gutierrez, Journal of Electroanalytical Chemistry 495 (2000) 71.
[49]  Y.Y. Feng, L.X. Bi, Z.H. Liu, D.S. Kong, Z.Y. Yu, Journal of Catalysis 290 (2012) 18.
[50]  Q.W. Tang, L.H. Jiang, J. Qi, Q. Jiang, S.L. Wang, G.Q. Sun, Applied Catalysis B: Environmental 104 (2011) 337.